Supplemental Material: Controlling Matter Phases Beyond Markov

Baptiste Debecker, John Martin, François Damanet

Institut de Physique Nucléaire, Atomique et de Spectroscopie,
CESAM, University of Liège, B-4000 Liège, Belgium

This Supplemental Material provides analytical and numerical details on the results presented in the main text of "Controlling Matter Phases Beyond Markov". In Sec. I we provide details on the first example investigated in the main text: the 1$^{\text{st}}$-order DPT in the Lipkin-Meshkov-Glick model. We first discuss different descriptions of the system according to different approximations, such as a spin-only description after adiabatic elimination of the pseudomode. Then, we present the mean-field analysis of the spin and of the full (exact) model. We finish the section with the study of the impact of the reservoir parameters on the position of the critical point. Finally, in Sec. II, we present the mean-field analysis of the second example investigated in the main text: the 2$^{\text{nd}}$-order DPTs in the extended LMG model.

I. FIRST MODEL - SHIFTING PHASE BOUNDARIES VIA NON-MARKOVIAN EFFECTS

In this section, we present details on the first model we consider in the main text, i.e., the generalized dissipative Lipkin-Meshkov-Glick model, which generalizes the study made in Ref. [S1] to the non-Markovian regime. The master equation for the collective spin and pseudomode density matrix reads [Eq. (8) in the main text]

$$
\dot{\rho}_{\text{tot}} = -i\left[H, \rho_{\text{tot}}\right] + \kappa \left(2a\rho_{\text{tot}}a^\dagger - \{a^\dagger a, \rho_{\text{tot}}\}\right)
$$
$$
\text{with} \qquad H = H_{\text{LMG}} + \omega a^\dagger a + \sqrt{\frac{\gamma\kappa}{2N}}\left(S_- a^\dagger + a S_+\right). \tag{S1}
$$

In the following, we first show how adiabatic elimination of the cavity mode recovers the original model [Eq.(7) in the main text] in the "bad cavity" limit before performing a mean-field analysis of our generalized model.

A. Adiabatic elimination of the cavity mode in the bad cavity limit

Let us perform a standard derivation of a master equation for the collective spin only, first dividing $H = H_0 + H_1$ and then working in the interaction picture with respect to $H_0 = H_{\text{LMG}} + \omega a^\dagger a$. In this interaction picture, the interaction Hamiltonian H_1 takes the form:

$$
H_1(t) = \sqrt{\frac{\gamma\kappa}{2N}}(a(t)S_+(t) + a^\dagger(t)S_-(t)), \tag{S2}
$$

where $S_\pm(t) = e^{iH_{\text{LMG}}t}S_\pm e^{-iH_{\text{LMG}}t}$. The master equation for the collective spin density operator $\rho = \text{Tr}_E(\rho_{\text{tot}})$ reads in the Markov approximation [S2]:

$$
\dot{\rho} = -\int_0^t dt' \text{Tr}_E\left([H_1(t), [H_1(t'), \rho_{\text{tot}}(t)]]\right). \tag{S3}
$$

Considering the Born approximation $\rho_{\text{tot}}(t) \approx \rho(t) \otimes \rho_E$ with ρ_E the vacuum state for the pseudomode and expanding the double commutator yields

$$
\dot{\rho} = -\int_0^t dt' \Big(\alpha(t-t')S_+(t)S_-(t')\rho(t) - \alpha^*(t-t')S_-(t)\rho(t)S_+(t') - \alpha(t-t')S_-(t')\rho(t)S_+(t) + \alpha^*(t-t')\rho(t)S_+(t')S_-(t)\Big), \tag{S4}
$$

which made appear the bath correlation function

$$
\alpha(t-t') = \left(\frac{\gamma\kappa}{2N}\right)\text{Tr}_E\left(a(t)a^\dagger(t')\rho_E\right) = \frac{\gamma\kappa}{2N}e^{-i\omega(t-t')-\kappa|t-t'|}. \tag{S5}
$$

a. "Bad cavity" limit $\kappa \to \infty$. In the "bad cavity" limit $\kappa \to \infty$, which corresponds to the case of a flat spectral density of the bath, we have $\alpha(t - t') \to (\gamma/N)\delta(t - t')$, which makes it possible to perform the integration straightforwardly and obtain the following master equation in the Schrödinger picture

$$\dot{\rho} = -i\,[H_{\mathrm{LMG}}, \rho] + \frac{\gamma}{2N}\,(2S_-\rho S_+ - \{S_+ S_-, \rho\})\,, \tag{S6}$$

which is exactly Eq. (7) in the main text.

b. Finite κ *and large detuning limit.* If we know consider the case of finite κ, the integrand in Eq. (S4) is now non-zero over a finite range of time t', so that one has in principle to know the explicit time-dependence of the system operators $S \pm (t') = e^{iH_{\mathrm{LMG}}t}S_\pm e^{-iH_{\mathrm{LMG}}t}$ - and thus the H_{LMG} Hamiltonian spectrum – to perform the integral. Such knowledge is however not needed in the limit where the pseudomode frequency ω dominates all system transition frequencies as shown below. Suppose indeed a spectral decomposition of H_{LMG} of the form $H_{\mathrm{LMG}}|n\rangle = \omega_n|n\rangle$ with eigenvalues and eigenvectors ω_n and $|n\rangle$. The time-dependence of the system operators $S_\pm(t')$ in the H_{LMG} Hamiltonian basis reads

$$S_\pm(t) = \sum_{n,n'} e^{-i(\omega_n - \omega_{n'})t} \langle n|S_\pm|n'\rangle |n\rangle\langle n'|. \tag{S7}$$

Inserting Eq. (S7) in Eq. (S4), making the variable substitution $t' \to t - \tau$ and pushing the limit of the integral to infinity yields after integration

$$
\begin{aligned}
\dot{\rho} = -\frac{\gamma\kappa}{2N} \sum_{n,n'} \Big(& \frac{1}{\kappa + i(\omega - (\omega_n - \omega_{n'}))} S_+(t) \left(e^{-i(\omega_n - \omega_{n'})t} \langle n|S_-|n'\rangle |n\rangle\langle n'| \right) \rho(t) \\
& - \frac{1}{\kappa - i(\omega + (\omega_n - \omega_{n'}))} S_-(t)\rho(t) \left(e^{-i(\omega_n - \omega_{n'})t} \langle n|S_+|n'\rangle |n\rangle\langle n'| \right) \\
& - \frac{1}{\kappa + i(\omega - (\omega_n - \omega_{n'}))} \left(e^{-i(\omega_n - \omega_n')t} \langle n|S_-|n'\rangle |n\rangle\langle n'| \right) \rho(t)S_+(t) \\
& + \frac{1}{\kappa - i(\omega + (\omega_n - \omega_{n'}))} \rho(t) \left(e^{-i(\omega_n - \omega_{n'})t} \langle n|S_+|n'\rangle |n\rangle\langle n'| \right) S_-(t) \Big).
\end{aligned} \tag{S8}
$$

If now we have $\omega \gg (\omega_n - \omega_{n'}) \,\forall n, n'$, then $1/(\kappa \pm i(\omega \pm (\omega_n - \omega_{n'})) \approx 1/(\kappa \pm i\omega)$ and the equation becomes

$$\dot{\rho} = -\frac{\gamma\kappa}{2N} \Big(\frac{1}{\kappa + i\omega} S_+(t)S_-(t)\rho(t) - \frac{1}{\kappa - i\omega} S_-(t)\rho(t)S_+(t) - \frac{1}{\kappa + i\omega} S_-(t)\rho(t)S_+(t) + \frac{1}{\kappa - i\omega}\rho(t)S_+(t)S_-(t) \Big). \tag{S9}$$

Coming back to the Schrödinger picture yields

$$\dot{\rho} = -i\left[H_{\mathrm{LMG}} - q_2 \frac{\gamma}{2N}S_+ S_-, \rho \right] + q_1 \frac{\gamma}{2N}\,(2S_-\rho S_+ - \{S_+ S_-, \rho\})\,, \tag{S10}$$

where we introduced the factors

$$q_1 = \frac{\kappa^2}{\kappa^2 + \omega^2}, \qquad q_2 = \frac{\kappa\omega}{\kappa^2 + \omega^2}. \tag{S11}$$

Hence, we see that in the large detuning limit $\omega/(\omega_n - \omega_{n'}) \to \infty \,\forall n, n'$, the structure of the bath spectral density has the effect of reducing the impact of the dissipative part of the master equation for the spin by a factor $q_1 = \kappa^2/(\kappa^2 + \omega^2)$ as well as adding a energy shift proportional to $q_2\gamma/2N$.

c. Redfield master equation. As explained above, going beyond the approximations used in the previous section require to take into account the spectrum of the system to evaluate the dissipative part of the master equation. However, the Lipkin-Meshkov-Glick Hamiltonian has complicated eigenvalues and eigenvectors [S3, S4] and it is not easy to write down simple formula for Eq. (S7), which hampers the writing of a simple expression for the master equation and stongly motivates the use of our systematic HEOM approach.

B. Mean-field analysis

We first start by writing the Heisenberg equations of motion for a, S_x, S_y and S_z from Eq. (S1)

$$
\begin{aligned}
\dot{a} &= -(\kappa + i\omega)a - i\sqrt{\frac{\gamma\kappa}{2N}}S_-, \\
\dot{S}_x &= -\frac{V}{N}\{S_y, S_z\} + i\sqrt{\frac{\gamma\kappa}{2N}}S_z(a - a^\dagger), \\
\dot{S}_y &= -\frac{V}{N}\{S_x, S_z\} - \sqrt{\frac{\gamma\kappa}{2N}}S_z(a + a^\dagger), \\
\dot{S}_z &= 2\frac{V}{N}\{S_x, S_y\} + i\sqrt{\frac{\gamma\kappa}{2N}}\left(a^\dagger S_- - aS_+\right).
\end{aligned}
\tag{S12}
$$

Using $\langle AB \rangle = \frac{1}{2}\langle\{A, B\} + [A, B]\rangle \approx \langle A\rangle\langle B\rangle + \frac{1}{2}\langle[A, B]\rangle$, we get the mean-field semiclassical equations of motion

$$
\langle\dot{a}\rangle = -(\kappa + i\omega)\langle a\rangle - i\sqrt{\frac{\gamma\kappa}{2N}}\langle S_-\rangle,
\tag{S13}
$$

$$
\langle\dot{S}_x\rangle = -2\frac{V}{N}\langle S_y\rangle\langle S_z\rangle + i\sqrt{\frac{\gamma\kappa}{2N}}\langle S_z\rangle(\langle a\rangle - \langle a^\dagger\rangle),
\tag{S14}
$$

$$
\langle\dot{S}_y\rangle = -2\frac{V}{N}\langle S_x\rangle\langle S_z\rangle - \sqrt{\frac{\gamma\kappa}{2N}}\langle S_z\rangle(\langle a\rangle + \langle a^\dagger\rangle),
\tag{S15}
$$

$$
\langle\dot{S}_z\rangle = 4\frac{V}{N}\langle S_x\rangle\langle S_y\rangle + i\sqrt{\frac{\gamma\kappa}{2N}}(\langle a^\dagger\rangle\langle S_-\rangle - \langle a\rangle\langle S_+\rangle),
\tag{S16}
$$

which are exact in the thermodynamic limit $N \to \infty$. Note that the quantity $\langle S_x\rangle^2 + \langle S_y\rangle^2 + \langle S_z\rangle^2$ is a constant of motion, hence the dynamics of the spin is constrained to the surface of a Bloch sphere. In the following, we are interested in finding the fixed points of these equations and studying their stability as a function of the parameters of the model, in order to deduce the different possible steady states and build a phase diagram as in [S1].

The different fixed points labelled as $\{(\langle a\rangle, \langle S_x\rangle, \langle S_y\rangle, \langle S_z\rangle)_*\}$ of Eqs. (S13)-(S16) can be obtained by setting the left-hand-side of all the equations to zero. In particular, from the first equation, setting $\langle\dot{a}\rangle = 0$ gives

$$
\langle a\rangle_* = -i\frac{\sqrt{\frac{\gamma\kappa}{2N}}\langle S_-\rangle_*}{\kappa + i\omega}
\tag{S17}
$$

Hence, the pseudomode degree of freedom is slaved to the collective spin ones, which simplifies the problem as we just need to find first the fixed points of a closed set of equations for the collective spin variables $\langle S_x\rangle_*$, $\langle S_y\rangle_*$ and $\langle S_z\rangle_*$ only, i.e.,

$$
0 = -2\frac{V}{N}\langle S_y\rangle_*\langle S_z\rangle_* + \frac{\gamma}{N}\langle S_z\rangle_*\left(q_1\langle S_x\rangle_* - q_2\langle S_y\rangle_*\right),
\tag{S18}
$$

$$
0 = -2\frac{V}{N}\langle S_x\rangle_*\langle S_z\rangle_* + \frac{\gamma}{N}\langle S_z\rangle_*\left(q_1\langle S_y\rangle_* + q_2\langle S_x\rangle_*\right),
\tag{S19}
$$

$$
0 = 4\frac{V}{N}\langle S_x\rangle_*\langle S_y\rangle_* - \frac{\gamma}{N}q_1\left(\langle S_x\rangle_*^2 + \langle S_y\rangle_*^2\right).
\tag{S20}
$$

It is worth noting that if one is interested in deriving a spin-only description of the model by performing an adiabatic elimination of the pseudomode (as done in the case of the Dicke model in [S5]), it would also require to setting $\dot{a} = 0$ in Eqs. (S13)-(S16), which would yield Eqs. (S18)-(S20) but with the derivative of the collective spin operators on the left-hand-sides of each equation. Importantly, this means the fixed points of the spin system after adiabatic elimination of the pseudomode are the same as the full model. However, as we will see below, their stability differs depending on whether or not we account for the pseudomode degree of freedom. Note also that taking the limit $\kappa/\omega \to \infty$ in Eqs. (S18)-(S20) yields $q_1 \to 1$ and $q_2 \to 0$, so that we recover the semiclassical equations of the Lindblad model [S1].

Equations (S18)-(S20) together with the normalization condition $\langle S_x\rangle_*^2 + \langle S_y\rangle_*^2 + \langle S_z\rangle_*^2 = (N/2)^2$ admit (as for the Markovian case) two classes of fixed points:

$$
(\langle S_x\rangle, \langle S_y\rangle, \langle S_z\rangle)_* = \frac{N}{2}(0, 0, \pm 1)
\tag{S21}
$$

and

$$\left(\langle S_x\rangle, \langle S_y\rangle, \langle S_z\rangle\right)_* = \frac{N}{2}\left(\frac{\sqrt{1\pm\sqrt{1-\frac{q_1^2\gamma^2}{4V^2}}}}{\sqrt{2}}, \frac{q_1\gamma}{4V}\frac{\sqrt{2}}{\sqrt{1\pm\sqrt{1-\frac{q_1^2\gamma^2}{4V^2}}}}, 0\right),\tag{S22}$$

$$\left(\langle S_x\rangle, \langle S_y\rangle, \langle S_z\rangle\right)_* = -\frac{N}{2}\left(\frac{\sqrt{1\pm\sqrt{1-\frac{q_1^2\gamma^2}{4V^2}}}}{\sqrt{2}}, \frac{q_1\gamma}{4V}\frac{\sqrt{2}}{\sqrt{1\pm\sqrt{1-\frac{q_1^2\gamma^2}{4V^2}}}}, 0\right).\tag{S23}$$

According to Eq. (S17), the first class of fixed points corresponds to the spin at the north and south poles of the Bloch sphere with an empty pseudomode, while the second class of fixed points corresponds to the spin at four different locations at the equator and a scaling $\langle a\rangle_* \propto \sqrt{N}$ for the pseudomode. In the following, we analyse the stability of these fixed points to determine the steady states of the model. As it turns out that it depends on whether the analysis is performed on the spin degrees of freedom (S_x, S_y, S_z) only (spin model), as obtained from adiabatic elimination of the pseudomode, or on all degrees of freedom (a, S_x, S_y, S_z) (full model), we investigate subsequently these two cases.

1. Spin model

a. Linear stability analysis. Let us first perform a linear stability analysis for the spin model obtained after adiabatic elimination of the pseudomode, i.e.,

$$\langle \dot{S}_x\rangle = -2\frac{V}{N}\langle S_y\rangle\langle S_z\rangle + \frac{\gamma}{N}\langle S_z\rangle\left(q_1\langle S_x\rangle - q_2\langle S_y\rangle\right),\tag{S24}$$

$$\langle \dot{S}_y\rangle = -2\frac{V}{N}\langle S_x\rangle\langle S_z\rangle + \frac{\gamma}{N}\langle S_z\rangle\left(q_1\langle S_y\rangle + q_2\langle S_x\rangle\right),\tag{S25}$$

$$\langle \dot{S}_z\rangle = 4\frac{V}{N}\langle S_x\rangle\langle S_y\rangle - \frac{\gamma}{N}q_1\left(\langle S_x\rangle^2 + \langle S_y\rangle^2\right),\tag{S26}$$

around the first class of fixed points: $(\langle S_x\rangle, \langle S_y\rangle, \langle S_z\rangle)_* = (0, 0, \pm N/2)$. Note that the equations above can also be obtained from the master equation (S10) in the large detuning limit. To perform the analysis, we replace $(\langle S_x\rangle, \langle S_y\rangle, \langle S_z\rangle)$ by $(x, y, z\pm(N/2))$ in Eqs. (S24-S26) where (x, y, z) denotes fluctuations around the fixed points which yields

$$\dot{x} = -2\frac{V}{N}y\left(z\pm\frac{N}{2}\right) + \frac{\gamma}{N}\left(z\pm\frac{N}{2}\right)\left(q_1 x - q_2 y\right),\tag{S27}$$

$$\dot{y} = -2\frac{V}{N}x\left(z\pm\frac{N}{2}\right) + \frac{\gamma}{N}\left(z\pm\frac{N}{2}\right)\left(q_1 y + q_2 x\right),\tag{S28}$$

$$\dot{z} = 4\frac{V}{N}xy - \frac{\gamma}{N}q_1\left(x^2 + y^2\right).\tag{S29}$$

Linearizing Eqs. (S27)-(S29) shows that fluctuations along z decouple from those along x and y, which reduces the analysis to the following two-dimensional system

$$\begin{pmatrix}\dot{x}\\\dot{y}\end{pmatrix} = \pm\frac{\gamma}{2}\begin{pmatrix}q_1 & -\frac{2V}{\gamma}-q_2\\-\frac{2V}{\gamma}+q_2 & q_1\end{pmatrix}\begin{pmatrix}x\\y\end{pmatrix}.\tag{S30}$$

The eigenvalues of the matrix are $\pm\gamma(q_1 - \sqrt{4(V/\gamma)^2 - q_2^2})/2$ and $\pm\gamma(q_1 + \sqrt{4(V/\gamma)^2 - q_2^2})/2$. For the fixed point $(\langle S_x\rangle, \langle S_y\rangle, \langle S_z\rangle)_* = \left(0, 0, \frac{N}{2}\right)$ ["+" sign in Eq. (S30)], the eigenvalue $\gamma(q_1 + \sqrt{4(V/\gamma)^2 - q_2^2})/2$ is always positive, meaning that the fixed point is always unstable. For the fixed point $(\langle S_x\rangle, \langle S_y\rangle, \langle S_z\rangle)_* = \left(0, 0, -\frac{N}{2}\right)$ ["–" sign in Eq. (S30)], both the eigenvalues $-\gamma(q_1 - \sqrt{4(V/\gamma)^2 - q_2^2})/2$ and $-\gamma(q_1 + \sqrt{4(V/\gamma)^2 - q_2^2})/2$ are negative for

$$V < \frac{\gamma}{2\sqrt{1+\omega^2/\kappa^2}} \equiv V_c^+,\tag{S31}$$

and $-\gamma(q_1 - \sqrt{4(V/\gamma)^2 - q_2^2})/2$ is positive for $V > V_c^+$. Hence, the fixed point $(\langle S_x\rangle, \langle S_y\rangle, \langle S_z\rangle)_* = \left(0, 0, -\frac{N}{2}\right)$ is stable only if $V < V_c^+$ and unstable otherwise. Note again that in the limit $\kappa/\omega \to \infty$, we recover the result of the Lindblad model of [S1] where $V_c^+ \to \gamma/2$.

Let us now perform a linear stability analysis around the second class of fixed points of the form $(\langle S_x \rangle, \langle S_y \rangle, \langle S_z \rangle)_* = (s_{x*}, s_{y*}, 0)$, where s_{x*} and s_{y*} are given by the right-hand side of Eqs. (S22) or (S23). Here, the EOM for the fluctuations, obtained by replacing $(\langle S_x \rangle, \langle S_y \rangle, \langle S_z \rangle)$ by $(x + s_{x*}, y + s_{y*}, z)$, yields after linearization

$$
\begin{pmatrix} \dot{x} \\ \dot{y} \\ \dot{z} \end{pmatrix} = \frac{1}{N} \begin{pmatrix} 0 & 0 & q_1 \gamma s_{x*} - (2V + q_2 \gamma) s_{y*} \\ 0 & 0 & q_1 \gamma s_{y*} - (2V - q_2 \gamma) s_{x*} \\ 4V s_{y*} - 2q_1 \gamma s_{x*} & 4V s_{x*} - 2q_1 \gamma s_{y*} & 0 \end{pmatrix} \begin{pmatrix} x \\ y \\ z \end{pmatrix} + \begin{pmatrix} 0 \\ 0 \\ -\frac{N \gamma q_1}{4} \end{pmatrix}. \tag{S32}
$$

The eigenvalues of the matrix are

$$
0, \quad -N \sqrt{ \left(\pm q_2 \sqrt{4V^2 - \gamma^2 q_1^2} + \gamma^2 q_1^2 - 4V^2 \right)/2 }, \quad \text{and} \quad N \sqrt{ \left(\pm q_2 \sqrt{4V^2 - \gamma^2 q_1^2} + \gamma^2 q_1^2 - 4V^2 \right)/2 }, \tag{S33}
$$

where the $\pm$ sign relate to the $\pm$ sign in Eqs. (S22) and (S23). Note that the zero eigenvalue is not physical, as the variables are not independent. To see how this eigenvalue can be eliminated, one can switch to the spherical coordinates $\langle S_x \rangle = r \sin \theta \cos \varphi$, $\langle S_y \rangle = r \sin \theta \sin \varphi$, $\langle S_z \rangle = r \cos \theta$ in Eqs. (S24-S26), which yields $\dot{r} = 0$ because of the norm conservation and

$$
\dot{\varphi} = \frac{\cos \theta}{2} \left[q_2 \gamma - 2V \cos(2\varphi) \right], \tag{S34}
$$

$$
\dot{\theta} = \frac{\sin \theta}{2} \left[q_1 \gamma - 2V \sin(2\varphi) \right]. \tag{S35}
$$

Linear stability analysis based on these equations yields the two non-trivial eigenvalues of Eq. (S33). The fixed points are unstable when the real part of at least one of them is positive. This happens for

$$
V < \frac{\gamma}{2 \left(1 + \omega^2/\kappa^2 \right)} \equiv V_c^- \tag{S36}
$$

for the two fixed points associated with the "–" sign in Eqs. (S22) and (S23) and for

$$
V < V_c^+ \tag{S37}
$$

for the two fixed points associated with the "+" sign. Above these critical values, the real part of both the eigenvalues are zero, and so one cannot conclude on the stability of the fixed points in this region via this simple linear stability analysis.

While the approach above cannot provide a full understanding of the stability of the system, we already see strong deviations from the Markovian limit $\omega/\kappa \to 0$. Indeed, in this latter, we have $V_c^- = V_c^+ = V_c^M = \gamma/2$ so that there is no region of parameters where the two kind of fixed points are not unstable, hampering the possibility for a coexistence of two distinct phases. More specifically, in [S1], it was shown that for $V < V_c^M$ the fixed point $(0, 0, -N/2)$ is the unique steady state while for $V > V_c^M$ the fixed points $(s_{x*}, s_{y*}, 0)$ are center fixed points and there exists an infinite set of oscillating (initial-state-dependent) steady states corresponding to orbits around these fixed points on the Bloch sphere. While these steady states are persistent spin oscillations, they average to zero along the z direction over time, so that the Markovian scenario well-describes a 1$^{\text{st}}$-order transition between a phase with $\langle S_z \rangle \neq 0$ ($V < V_c^M$) and $\langle S_z \rangle = 0$ ($V > V_c^M$). In the case $\omega/\kappa \neq 0$, however, we have $V_c^- < V_c^+$, so the possibility that the fixed points and thus two distinct phases coexist in the region $V_c^- < V < V_c^+$ (which increases as ω/κ increases) is not excluded. This is confirmed in the next subsection.

b. Higher-order stability analysis. As the equations of motion are cumbersome beyond linearization, we rely on a numerical analysis of the stability of the fixed points, as summarized below.

For $0 \leq V < V_c^-$, the fixed point $(0, 0, -N/2)$ is the unique steady state, as shown in the stream plots in Fig. S1 (a,b,e). Note that in this regime all the fixed points of the form $(s_{x*}, s_{y*}, 0)$ are not physical fixed points as they are complex vectors.

For $V_c^- < V < V_c^+$, we observe a bistability phenomenon as the steady state depends on the initial conditions: the fixed point $(0, 0, -N/2)$ is still a possible steady state, but an infinite number of steady states corresponding to stable orbits on the Bloch sphere around the two center fixed points (S22) and (S23) with the "–" sign become available, as shown in Fig. S1(f). For $V \gtrsim V_c^-$, only orbits close to the fixed points are stable. As V increases, more orbits become stable. This is in sharp contrast with the Markovian case where all the points on the sphere belong to stable orbits as soon as $V > V_c^M$ [panel (c,d)]. Here, in the regime $V_c^- < V < V_c^+$, each point on the Bloch sphere undergoes the phase transition at a different critical point.

For $V > V_c^+$, the fixed point $(0, 0, -N/2)$ is no longer stable and all the four fixed points (S22) and (S23) become center fixed points, as can be seen in Fig. S1(g,h). Note that since $V_c^+ < V_c^M$, this means going beyond the limit of a
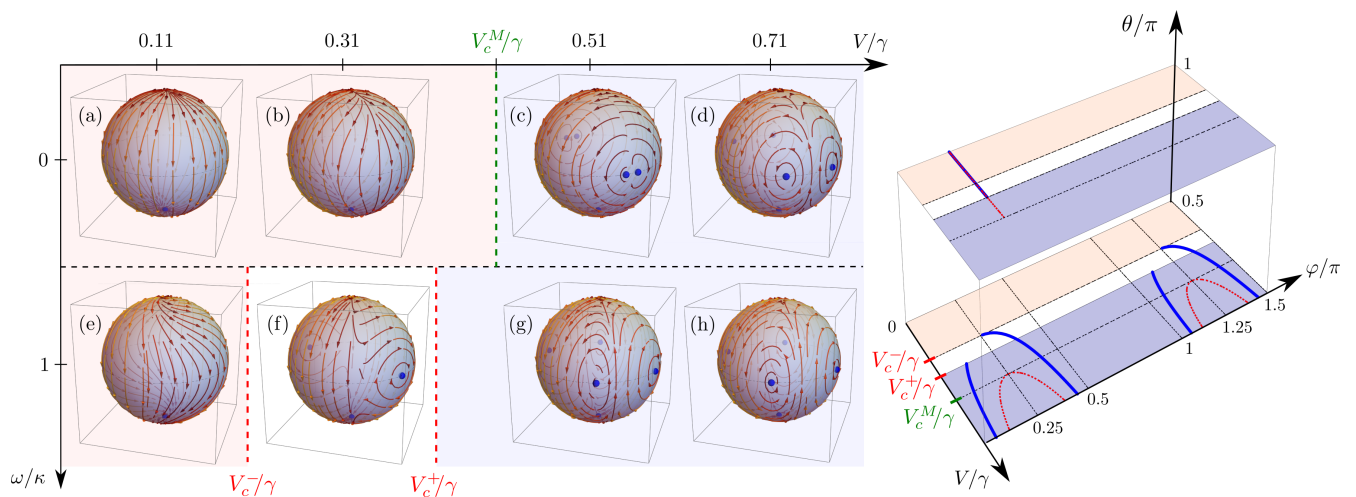
FIG. S1. Stream plots obtained from the mean-field equations (S24)-(S26) after adiabatic elimination of the pseudomode showing the trajectories of the collective spin on the Bloch sphere in the thermodynamic limit as a function of the ratio V/γ between coherent and dissipative rates (not in scale) and of the degree of spectral density structures ω/κ. In the Markovian limit ($\omega/\kappa \to 0$), there is a phase transition at $V = V_c^M = \gamma/2$ between a phase with a unique pure steady state $(0, 0, -N/2)$ (blue dot at the south pole) [$V < V_c^M$, (a,b)] and a phase with an infinite set of (initial-state-dependent) pure steady states orbiting around four center fixed points (blue dots at the equator) [$V > V_c^M$, (c,d)]. As ω/κ increases, the stream lines twist around the z-axis (e) and a region of parameters ($V_c^- < V < V_c^+$) emerges where both the steady state $(0, 0, -N/2)$ or a steady orbit can be observed depending on the initial condition (f). Overall, the phase space where the coherent dynamics dominates over the dissipative one is enlarged due to non-Markovian effects. Parameters are $V/\gamma = 0.11$ (a,e), $V/\gamma = 0.31$ (b,f), $V/\gamma = 0.51$ (c,g) and $V/\gamma = 0.71$ (d,h). For $\omega/\kappa = 1$, $V_c^-/\gamma = 0.25$ and $V_c^+/\gamma \approx 0.354$. (i) Positions of the relevant fixed points on the Bloch sphere as a function of spherical coordinates φ and θ and V/γ for the Markovian limit $\omega/\kappa = 0$ (dashed red) and for $\omega/\kappa = 1$ (blue).

flat spectral density has the effect to renormalize to lower values the critical point by a function of the bath SD. We interpret this phenomenon as a consequence of memory effects: for smaller κ/ω, the excitations escaping the system are more likely to be re-absorbed by the system at later times, protecting its coherence and hence stabilizing the phase dominated by the Hamiltonian term to lower ratio V/γ.

2. Full model

We now come back to the mean-field equations for the full model (S13)-(S16) in order to study how reintroducing the pseudomode degree of freedom affects the stability of the fixed points. Here, the complex variable $\langle a \rangle$ can be decomposed into two real variables. Hence, the linear stability analysis on the full model exhibits four non-trivial eigenvalues to analyze, by contrast with the two of the previous section. As before, the analysis consists in linearizing the equations of motion for the fluctuations around the different fixed points and inspecting the eigenvalues of the matrix of the system. We summarize below the results for each class of fixed points.

For the first class of fixed points at the north and south poles of the Bloch sphere, $(\langle S_x \rangle_*, \langle S_y \rangle_*, \langle S_z \rangle_*) = (0, 0, N/2)$ is still unstable for all values of V, while $(0, 0, -N/2)$ is still a valid steady state for $V < V_c^+$, as can be seen in panel (a) and (b) respectively of Fig. S2, which displays the real parts of the eigenvalues of the linear stability analysis matrix in each case.

For the second class of fixed points at the equator of the Bloch sphere, the changes are more drastic. (i) The two fixed points associated with the "−" sign in Eqs. (S22) and (S23) are still unstable for $V < V_c^-$. However, they are now *stable* for $V > V_c^-$, as can be seen in Fig. S2(c) showing that all real parts of the eigenvalues become negative in this region (blue solid curve), by contrast with the analysis of the reduced spin model (dashed purple and dotted dark cyan). Hence, these two fixed points are now real steady states for $V > V_c^-$, and they coexist with the steady state $(0, 0, -N/2)$ for $V_c^- < V < V_c^+$. There are no more stable orbits around these fixed points. (ii) The two fixed points associated with the "+" sign in Eqs. (S22) and (S23) are still unstable for $V < V_c^+$, and now become also unstable above V_c^+, as can be seen in Fig. S2(d).

In conclusion, the mean-field analysis of our generalized LMG model (S1) yields qualitatively different phase diagrams depending on the approximations used.
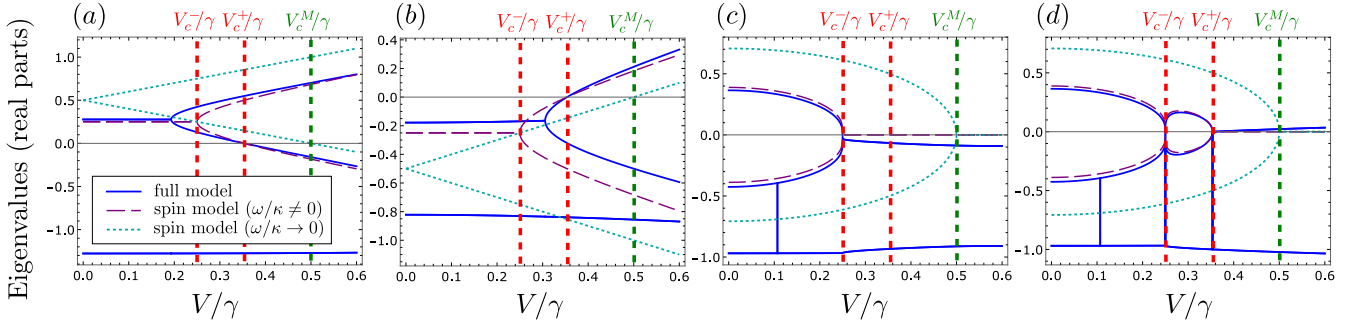
FIG. S2. Real parts of the eigenvalues of the linear stability analysis matrix of the mean-field equations for the full model [Eqs (S13)-(S16)] (blue solid lines) with $\omega = \kappa = \gamma$ and for the spin model after adiabatic elimination of the pseudomode [Eqs. (S24)-(S26)] (dashed purple lines) with $\omega = \kappa = \gamma$ and in the limit $\omega/\kappa \to 0$ (dotted dark cyan lines). The different panels correspond to linear stability analyses around different fixed points: at the north pole of the Bloch sphere $[(\langle S_x\rangle, \langle S_y\rangle, \langle S_z\rangle)_* = (0, 0, -N/2)]$ (a), at the south pole $[(0, 0, -N/2)]$ (b) and at the equators [Eqs. (S22)-(S23) with the "$-$" sign (c) and the "$+$" sign (d)]. For a given V/γ, the fixed points are stable if all the corresponding eigenvalues have a negative real parts, while they are unstable if at least one of them is positive. The vertical dashed lines indicate the positions of the special values of V/γ as described in the text.

- The original spin-only model of [S1] as obtained in the limit $\omega/\kappa \to 0$ exhibits the DPT at $V = V_c^M = \gamma/2$. For $V < \gamma/2$, $(0, 0, -N/2)$ is the only steady state, while for $V > \gamma/2$ they are four center fixed points at the equator of the Bloch sphere around which an infinity of stable orbits are valid steady states, which one is chosen depends on the initial conditions.

- When including the spectral structures of the bath in the reduced description of the spin system ($\omega/\kappa \neq 0$), the critical point is split into two: $V_c^- = \gamma/[2(1 + \omega^2/\kappa^2)]$ and $V_c^+ = \gamma/(2\sqrt{1 + \omega^2/\kappa^2})$ where $V_c^- < V_c^+$, and the four fixed points at the equator have shifted locations. For $V < V_c^-$, $(0, 0, -N/2)$ is the only steady state. For $V_c^- < V < V_c^+$, $(0, 0, -N/2)$ and an ensemble of stable orbits around two out of the four center fixed points can be steady states. For $V > V_c^+$, only stable orbits around the four center fixed points are steady states.

- In the exact full model, the fixed points remain the same but not their stability. Notably, stable orbit cannot be seen anymore in any regime. For $V < V_c^-$, $(0, 0, -N/2)$ is the only steady state. For $V_c^- < V < V_c^+$, $(0, 0, -N/2)$ and two fixed points at the equator can be steady states. For $V > V_c^+$, only these two latter can be steady states.

Signatures of this overall picture can be found within our HEOM approach, as it predicts for finite N a transition between V_c^- and V_c^+. We elaborate on this in the next section.

C. Impact of non-Markovianity on the critical point

In the main text, we showed that for the first LMG model we consider one can reshape the phase boundaries by considering a bath correlation function that decays with a finite time $1/\kappa$. In this section, we study more thoroughly the impact of this finite decay time on the DPT.

We find that the smaller κ/ω, the sharper the transition for a given N as illustrated by the panels (a)-(f) of Fig. S3. This result is not surprising as lowering κ/ω takes us further from the Markovian limit defined by $\kappa \to +\infty$, which in turn leads to larger values of $k_{\max}$ to ensure convergence. However, as $k_{\max}$ grows, the dimension of the HEOM Liouvillian $\mathcal{L}_{\mathrm{HEOM}}$ also increases, in close analogy with the thermodynamic limit $N \to +\infty$ which also increases the dimension of the HEOM Liouvillian. The panel (g) of Fig. S3 shows that the critical point, numerically extracted from $\mathcal{L}_{\mathrm{HEOM}}$ is always between V_c^+ and V_c^- for all values of κ/ω considered here, as expected. Furthermore, the critical point V_c/γ seems to more closely follow the scaling of V_c^+/γ given in Eq. (S31) than that of V_c^-/γ.

II. SECOND MODEL - TRIGGERING DPTS VIA NON-MARKOVIAN EFFECTS

This section is concerned with the second model considered in the main text, i.e., the modified LMG model coupled to a bath with exponentially decaying correlation function, which can be modelled as a spin system coupled to a damped pseudomode a.
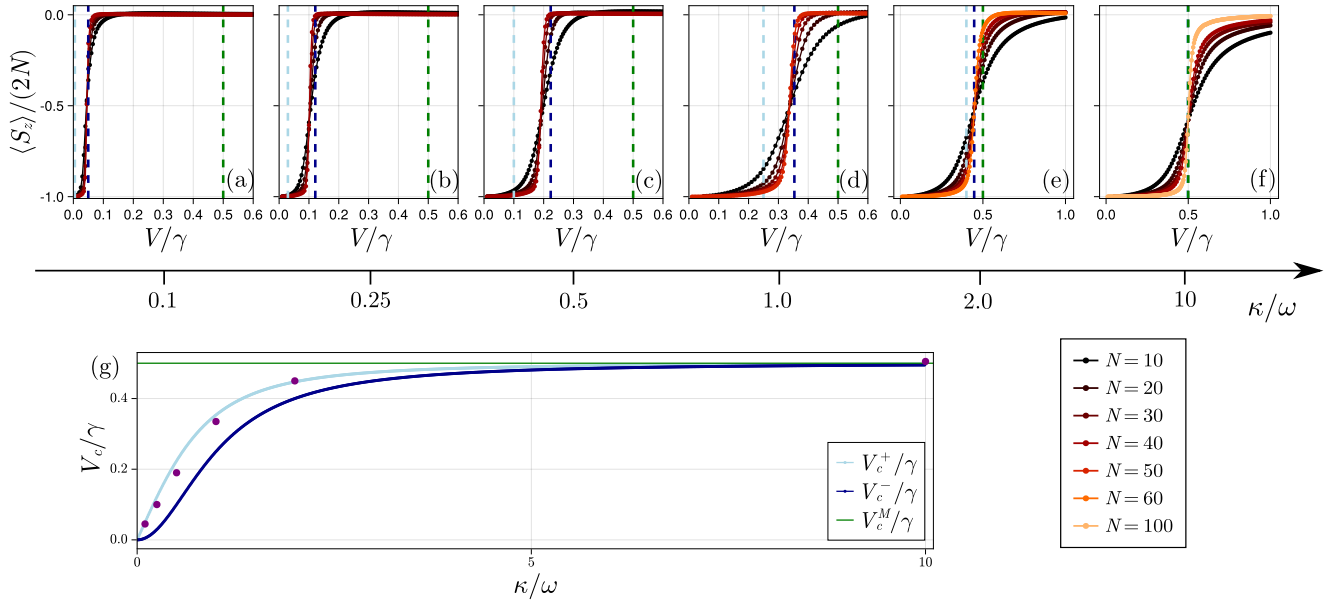
FIG. S3. Panels (a)-(f): Magnetization $\langle S_z \rangle /(2N)$ as a function of V/γ for different values of κ/ω [see axis below the plots] and for different values of N [see legend] highlighting the reshaping of the phase boundaries induced by non-Markovianity. Panel (g): Effective critical point V_c/γ (dots in purple), *i.e.* the critical point numerically found from $\mathcal{L}_{\text{HEOM}}$, as a function of κ/ω. We see that V_c/γ is always between $V_c^+\gamma$ and V_c^-/γ and appears to closely follow the scaling of V_c^+/γ given in Eq. (S31).

A. Mean-field analysis

In this section, we analyze the mean-field equations associated with the second model considered in the main text. The master equation for total density matrix reads

$$
\dot{\rho}_{\text{tot}} = -i[H, \rho_{\text{tot}}] + \kappa \left(2a\rho_{\text{tot}}a^\dagger - \{a^\dagger a, \rho_{\text{tot}}\} \right)
$$

$$
\text{with} \qquad H = H_{\text{LMG}} + hS_z + \omega a^\dagger a + \sqrt{\frac{\gamma\kappa}{2N}} S_x(a + a^\dagger).
\tag{S38}
$$

In close analogy with Section IV. B., it is easy to show that the mean-field equations read

$$
\langle \dot{a} \rangle = -(\kappa + i\omega)\langle a \rangle - i\sqrt{\frac{\gamma\kappa}{2N}}\langle S_x \rangle,
\tag{S39}
$$

$$
\langle \dot{S}_x \rangle = -2\frac{V}{N}\langle S_y \rangle \langle S_z \rangle - h\langle S_y \rangle,
\tag{S40}
$$

$$
\langle \dot{S}_y \rangle = -2\frac{V}{N}\langle S_x \rangle \langle S_z \rangle + h\langle S_x \rangle - \sqrt{\frac{\gamma\kappa}{2N}}\langle S_z \rangle(\langle a \rangle + \langle a^\dagger \rangle),
\tag{S41}
$$

$$
\langle \dot{S}_z \rangle = 4\frac{V}{N}\langle S_x \rangle \langle S_y \rangle + \sqrt{\frac{\gamma\kappa}{2N}}\langle S_y \rangle(\langle a \rangle + \langle a^\dagger \rangle).
\tag{S42}
$$

They have six fixed points from which four phases labelled as (I), (II), (IIb) and (III) can be inferred:

$$(\text{I}):\ (\langle a\rangle, \langle S_x\rangle, \langle S_y\rangle, \langle S_z\rangle)_* = \frac{N}{2}\left(\mp\sqrt{\frac{\gamma}{2N\kappa}}\sqrt{1-\left(\frac{h}{V-\frac{q_2\gamma}{2}}\right)^2}(q_2+iq_1), \pm\sqrt{1-\left(\frac{h}{V-\frac{q_2\gamma}{2}}\right)^2}, 0, \frac{h}{\left(V-\frac{q_2\gamma}{2}\right)}\right)$$

(S43)

$$(\text{II}):\ (\langle a\rangle, \langle S_x\rangle, \langle S_y\rangle, \langle S_z\rangle)_* = \frac{N}{2}\,(0,0,0,-1)$$

(S44)

$$(\text{IIb}):\ (\langle a\rangle, \langle S_x\rangle, \langle S_y\rangle, \langle S_z\rangle)_* = \frac{N}{2}\,(0,0,0,1)$$

(S45)

$$(\text{III}):\ (\langle a\rangle, \langle S_x\rangle, \langle S_y\rangle, \langle S_z\rangle)_* = \frac{N}{2}\left(0,0,\pm\sqrt{1-\left(\frac{h}{V}\right)^2}, -\frac{h}{V}\right).$$

(S46)

If $h>0$ ($h<0$), the phase (IIb) [(II)] is always unstable. As we chose $h>0$ in the main text, we thus only have the phases (I), (II), and (III) to consider. Phases (I) and (III) both gather two fixed points, corresponding in each case to two broken symmetry states. Also, we note that their fixed points are unphysical for $|V-q_2\gamma/2|<h$ and $|V|<h$, respectively, which already gives some hints about their stability. A linear stability analysis around the fixed points show that the phases are stable in distinct regions of parameters. For $h,q_2,\gamma>0$ as considered in the main text, we have the two critical points $V_1=\min\left(-h+\frac{q_2\gamma}{2}, \frac{q_2\gamma}{4}\right)$ and $V_2=\max\left(h, \frac{q_2\gamma}{4}\right)$ with phase (I) stable for $V<V_1$; phase (II) stable for $V_1<V<V_2$; and phase (III) stable for $V_2<V$. For $h>q_2\gamma/4$, the two critical points coalesce and phase (II) does not emerge anymore when varying V. In the particular case $\omega=\kappa=2\gamma=2h$ as considered in the main text, we have $V_1=-3\gamma/4$ and $V_2=\gamma$.

[S1] T. E. Lee, C.-K. Chan, and S. F. Yelin, Phys. Rev. A **90**, 052109 (2014).
[S2] H.-P. Breuer and F. Petruccione, *The Theory of Open Quantum Systems* (Oxford University Press, Oxford, 2006).
[S3] P. Ribeiro, J. Vidal, and R. Mosseri, Phys. Rev. E **78**, 021106 (2008).
[S4] N. Debergh and F. Stancu, Journal of Physics A: Mathematical and General **34**, 3265 (2001).
[S5] F. Damanet, A. J. Daley, and J. Keeling, Phys. Rev. A **99**, 033845 (2019).